International Journal of Biological Macromolecules 242 (2023) 124662

Contents lists available at ScienceDirect

International Journal of Biological Macromolecules

journal homepage: www.elsevier.com/locate/ijbiomac

A calorimetric and structural analysis of cooperativity in the thermal unfolding of the PDZ tandem of human Syntenin-1

Jose C. Martinez [a,*], Javier Ruiz-Sanz [a], María J. Resina [a], Fernando Montero [a], Ana Camara-Artigas [b], Irene Luque [a,*]

[a] Department of Physical Chemistry, Institute of Biotechnology and Excellence Unit in Chemistry Applied to Biomedicine and Environment, Faculty of Sciences, University of Granada, Avda. Fuentenueva, s/n, 18071 Granada, Spain
[b] Department of Chemistry and Physics, Agrifood Campus of International Excellence (ceiA3) and CIAMBITAL, University of Almería, Carretera de Sacramento s/n, 04120 Almería, Spain

ARTICLE INFO

Keywords:
Domains in tandem
Folding thermodynamics
Protein hydration

ABSTRACT

Syntenin-1 is a multidomain protein containing a central tandem of two PDZ domains flanked by two unnamed domains. Previous structural and biophysical studies show that the two PDZ domains are functional both isolated and in tandem, occurring a gain in their respective binding affinities when joined through its natural short linker. To get insight into the molecular and energetic reasons of such a gain, here, the first thermodynamic characterization of the conformational equilibrium of Syntenin-1 is presented, with special focus on its PDZ domains. These studies include the thermal unfolding of the whole protein, the PDZ-tandem construct and the two isolated PDZ domains using circular dichroism, differential scanning fluorimetry and differential scanning calorimetry. The isolated PDZ domains show low stability ($\Delta G < 10$ kJ·mol^{-1}) and poor cooperativity compared to the PDZ-tandem, which shows higher stability (20–30 kJ·mol^{-1}) and a fully cooperative behaviour, with energetics similar to that previously described for archetypical PDZ domains. The high-resolution structures suggest that this remarkable increase in cooperativity is associated to strong, water-mediated, interactions at the interface between the PDZ domains, associated to nine conserved hydration regions. The low T_m value (45 °C), the anomalously high unfolding enthalpy (>400 kJ·mol^{-1}), and native heat capacity values (above 40 kJ·K^{-1}·mol^{-1}), indicate that these interfacial buried waters play a relevant role in Syntenin-1 folding energetics.

1. Introduction

Even though small compact globular proteins typically exhibit extreme cooperativity, integrating the whole sequence into a single structural unit, larger proteins usually are arranged into structures composed of discrete structural domains that behave as individual cooperative modules. This modular architecture appears as a universal principle recurrently used by nature to construct large proteins. It can be justified by evolutionary reasons, since nature will prefer to design proteins by adapting pre-existing well-folded domains than following a *de novo* design process for every functional protein. Thermodynamics may also justify this option, since a protein should have a well-defined structure, stable enough to get over the thermal motion, R·T (being R the universal gas constant and T the absolute temperature), but the difficulties in organizing properly all the amino acids from the sequence into a unique, well-ordered, energetically optimized and cooperative structure increase dramatically with the sequence length. Furthermore, proteins should achieve a rapid self-assembling into their 3D structures [1] and, as a rule, one might assume that the occurrence of relatively stable folding intermediates should be avoided by evolution in most of the cases, as they could lead to biologically unwanted self-aggregation processes.

Hence, size is the key for modular disposition. Regardless of type and function, cooperative modular domains are generally limited in size, about 40 kDa, and in stability, with folding Gibbs energies typically below 60 kJ·mol^{-1} at 25 °C [2–4]. This limited stability (80 kJ·mol^{-1}) had been already postulated in the 1960s by Charles Tanford, on the basis of solubilities of amino acids and related substances in a variety of solvents by using pure thermodynamic and physical-chemical reasoning [5]. This limitation in stability would be dictated by biological

* Corresponding authors at: Department of Physical Chemistry, Faculty of Sciences, Avda. Fuentenueva, s/n, 18071 Granada, Spain.
E-mail addresses: jcmh@ugr.es (J.C. Martinez), jruizs@ugr.es (J. Ruiz-Sanz), mjresina@ugr.es (M.J. Resina), fmontero@ugr.es (F. Montero), acamara@ual.es (A. Camara-Artigas), iluque@ugr.es (I. Luque).

https://doi.org/10.1016/j.ijbiomac.2023.124662
Received 3 February 2023; Received in revised form 10 April 2023; Accepted 24 April 2023
Available online 27 April 2023

requirements such as functioning, turnover, or flexibility.

A very important advantage emerging from the modular arrangement is that the different domains constituting a given protein can cooperate to modify its functionality. It is well known, for instance, that tandems of PDZ domains achieve improved binding affinities with respect to the isolated domains. These features can enable regulatory mechanisms to control signalling events [6]. Moreover, alternative splicing is clearly favoured by multidomain organization, being highly beneficial, since it will increase multifunctionality at little cost [7]. The combination of energetic (folding/unfolding thermodynamics and kinetics) and structural studies is a powerful approach to distinguish whether different domains within a modular protein interact cooperatively or behave as independent units. Such studies, not only can inform on the degree of cooperativity gained upon covalent linkage of the domains, but also provide valuable information on the nature and magnitude of the contributions of the different types of interactions established at the interface [4]. Furthermore, the comparison of unfolding experiments between the tandem and its isolated structures will focus the energetic study at the domain interface, and/or at those regions responsible of the binding and unfolding cooperativity [8].

As mentioned above, a particularly interesting and frequent mode of multidomain organization in proteins is represented by tandem arrays of PDZ domains. In these cases, structurally homologous domains are presented in a contiguous assembly joined by a relatively short linker. Most of the PDZ domain-containing proteins are multimodular scaffold proteins comprising multiple PDZ domains, so that they can simultaneously interact with several binding partners and, thus, assemble supramolecular signalling complexes. The few existing studies on the folding/unfolding of different PDZ domains naturally ordered in a tandem disposition have revealed a wide range of alternatives, ranging from situations in which PDZ domains unfold independently [9–12] to others in which the domains behave as a single cooperative unit [8].

Syntenin-1 (also known as SDCBP) is a 32 kDa protein which sequence is highly conserved from vertebrates to arthropods. It functions as a multifunctional adapter protein, interacting primarily with membrane-bound proteins and being involved in the sub-cellular trafficking of various proteins to organize functional complexes during exocytosis and endocytosis [13]. Consequently, Syntenin-1 is implicated in important cellular events, such as receptor trafficking, regulation of neuronal architecture, synapse formation, axonal elongation, and exosome production. It also plays a role in the pathogenesis and metastasis of various cancers [14] and is a determining factor in the virulence of the SARS-CoV-2 infection [13,15].

From a structural point of view, Syntenin-1 contains a tandem of two PDZ domains in its central region flanked by two unnamed domains at the N- and C-termini [14]. The N-terminal domain has an autoinhibitory character, possibly regulated by Tyr phosphorylation [16], while the function of the C-terminal domain remains unknown, although it seems to be necessary for protein homo-dimerization [17]. PDZ domains are protein-protein interaction modules that normally contain six β strands and two α helices, and recognize C-terminal sequences in their targets, that fit in a binding groove conformed by the β2 strand and the α2 helix. Thus, the last four residues of the target C-terminal sequence bind as an additional β strand that interacts in an antiparallel orientation with respect to the β2 strand of the PDZ domain [18].

The PDZ domains mediate the interactions of human Syntenin with a variety of proteins [13]. They also bind the phospholipid phosphatidylinositol 4,5-bisphosphate (PIP2) as the 20 % of PDZ domains do [19]. Most interestingly, Syntenin interacts with the Envelope (E) protein of coronaviruses through a highly conserved -DLLV C-terminal motif. [20–23]. SARS-CoV-E is an integral membrane protein of about 76 amino acids, not constitutive of the virus, which accumulates in cells during infection. The elimination of SARS-CoV-E in animal models markedly reduces the massive expression of cytokines responsible for the acute respiratory process, increasing the possibility of survival [24–27]. In fact, a direct relationship between the SARS-CoV-E/Syntenin interaction and the activation of the p38 MAPK protein, responsible for the disproportionate increase in the expression of inflammatory cytokines during infection, has been established. Therefore, the SARS-CoV-E/Syntenin interaction plays a determining role in the severity and virulence of the infection and is a major target for broad-spectrum pharmacological intervention against coronaviruses, including SARS-CoV and SARS-CoV-2 variants [15,28].

In this work, the first thermodynamic characterization of the conformational equilibrium of Syntenin-1 is presented, with a special focus on its PDZ domains. Thermal unfolding experiments were carried out using circular dichroism (CD), differential scanning fluorimetry (DSF) and differential scanning calorimetry (DSC) of the full-length protein, the tandem of PDZ domains and the two isolated PDZ domains, under a variety of buffer conditions. The thermodynamic analysis of these experiments has revealed a cooperative interaction between both PDZ domains that might be well explained by a network of interactions, many of them mediated by occluded water molecules at the interface between the PDZ domains.

2. Results

2.1. Circular dichroism (CD) and differential scanning fluorimetry (DSF) analysis of the thermal unfolding of human Syntenin-1 and its fragments

Thermal denaturation experiments in different buffers, ionic strengths and pH conditions were performed with full-length Syntenin-1 in order to overcome its low solubility and identify the optimal conditions for its biophysical characterization (50 mM sodium phosphate, 500 mM sodium chloride, pH 7.5, referred to as TP6 from now on). In Fig. 1 the far-UV CD spectrum and the thermal unfolding profile of full-length human Syntenin-1 are shown, being the latter characterized by a single structural transition with a T_m value of 56 °C. Interestingly, the far-UV CD spectrum of full-length Syntenin-1 retains a significant level of ellipticity at high temperatures, suggesting that some degree of residual structure is preserved upon thermal unfolding. The irreversibility of the transition precluded a thorough thermodynamic analysis, although the sigmoidal shape of the thermal denaturation profile allows its fitting to a two-state model (see Materials and methods for details). The DSF thermal unfolding profiles of full-length Syntenin-1 show a similar behaviour, rendering comparable T_m values in PBS buffer (Fig. S1 and Table S1).

To improve solubility and reversibility in order to facilitate the thermodynamic characterization, the thermal unfolding of the Syntenin-1 PDZ tandem (residues 113–273, in the absence of the N- and C-terminal domains) was studied. The far-UV CD spectrum and thermal unfolding transition of the PDZ tandem (Fig. 1) are characterized by lower ellipticities in the 210–220 nm region compared to the full-length protein, indicating a loss in secondary structure that is well accounted for the removal of the N- and C-terminal domains, predicted to adopt helical structure in the AlphaFold model for full-length Syntenin-1 (PDB code: AF_AFO00560F1). The PDZ tandem construct shows a much higher solubility and partial reversibility, allowing for the thermodynamic analysis of the thermal denaturation transitions. The CD and DSF thermal unfolding experiments (Figs. 1 and S1, respectively) reveal a 10 °C decrease in the T_m value with respect to the full-length protein, with the unfolded state showing much less residual ellipticity.

The thermal unfolding of the Syntenin-1 PDZ tandem was studied under several conditions using different buffered solutions, pH values and ionic strengths. The experiments, which were performed in duplicate, allowed us to identify the conditions for optimal stability (highest T_m values) and reversibility (over 50 %): pH 7.0–8.0 with moderate-to-high ionic strength (Fig. S2). Fitting of the experimental traces to a two-state model resulted in T_m values of 41 °C at TP1 conditions and around 45-46 °C for TP2 to TP6. The van't Hoff unfolding enthalpies, reporting on the relative cooperativity of the transitions, were obtained, ranging between 600 kJ·mol^{-1} (under TP1 conditions) and 350 kJ·mol^{-1} (TP6

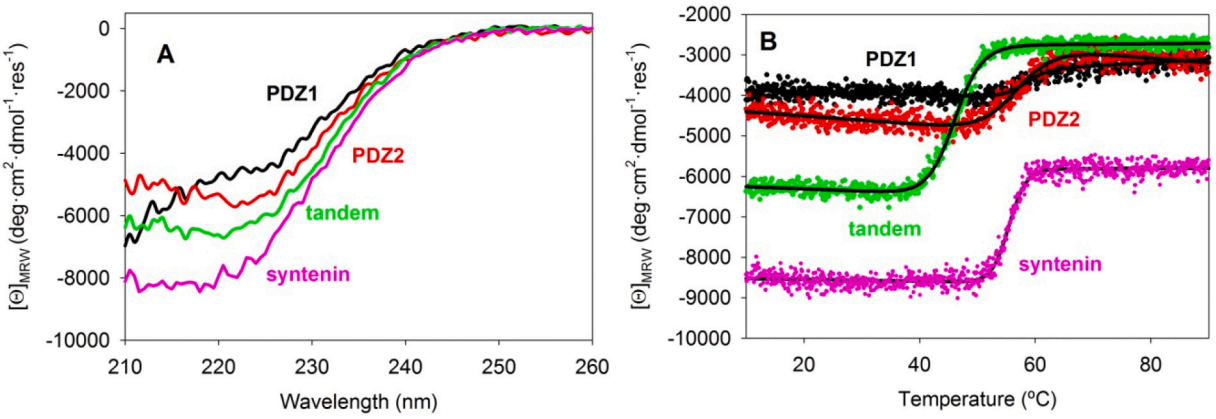

Fig. 1. **(A)** Far-UV CD spectra under TP6 conditions at 10 °C for full-length Syntenin-1 (pink), the PDZ1–2 tandem construct (green), and the isolated PDZ1 (black) and PDZ2 (red) domains. **(B)** Far-UV CD-thermal unfolding transitions corresponding to the thermal evolution of the molar ellipticity at 222 nm. Symbols correspond to the experimental data and black lines show the best fitting to a two-state model. Protein concentration was 30 μM for PDZ1, PDZ2 and PDZ tandem, and 10 μM for full-length Syntenin-1.

buffer). DSF experiments carried out in PBS buffer show a single unfolding transition (Fig. S1) rendering T_m values similar to those derived from the CD experiments under TP2 to TP6 conditions (Table S1).

Far-UV CD thermal unfolding experiments were also carried out with the two isolated PDZ domains (PDZ1 residues 113–193; PDZ2 residues 197–273) (Fig. 1). The isolated PDZ domains showed poor solubility that was optimal at TP6 conditions. Despite their partial reversibility (higher than 50 %), the CD spectra and the unfolding transitions of the isolated domains are clearly smaller in size (Fig. 1), suggesting a poor stability of the isolated domains in solution. As observed for the full-length protein, the ionic strength is clearly stabilizing these domains, which are almost unfolded in 40 mM sodium phosphate pH 7.0. Unfolding transitions displaying the highest T_m values were obtained under TP6 conditions (50 mM sodium phosphate 500 mM sodium chloride pH 7.5). Surprisingly, these T_m values are higher than that of the PDZ tandem and closer to the full-length protein values.

2.2. Differential scanning calorimetry (DSC) study of full-length human Syntenin-1

To perform a complete thermodynamic characterization of the unfolding equilibrium, the thermal unfolding of Syntenin-1 and the different PDZ constructs were studied by DSC. The DSC unfolding transition of the full-length protein was completely irreversible under all conditions studied; even when the first heating scan was stopped at the beginning of the heat evolution, no transition was recovered in the reheating scan. This precludes any further thermodynamic analysis. A small pre-transition appears in the unfolding traces of the full-length Syntenin-1 (Fig. 2) that is not found in the denaturation profiles of the PDZ tandem or the isolated PDZ domains. This pre-transition could be assigned to the unfolding of the N- and C-terminal domains, but the corresponding CD and DSF unfolding profiles show a single and well-defined S-shaped transition that coincides in T_m (around 55 °C) with the main endotherm observed in the DSC experiments (Figs. 1 and 2), ruling out this interpretation. Rather, considering that Syntenin-1 C-terminal domain seems to be implicated in protein homo-dimerization [17], this small pre-transition peak can be explained by the dissociation of oligomeric species into monomers, as previously described for other systems [29]. In any case, the poor solubility of full-length Syntenin-1 precluded a more thorough analysis of the protein concentration effects on thermal denaturation.

The DSC study of the PDZ tandem (comprising residues 113–273) confirms the ten-degree drop in T_m with respect to the full-length protein observed in the CD and DSF studies. Nonetheless, this loss in T_m is

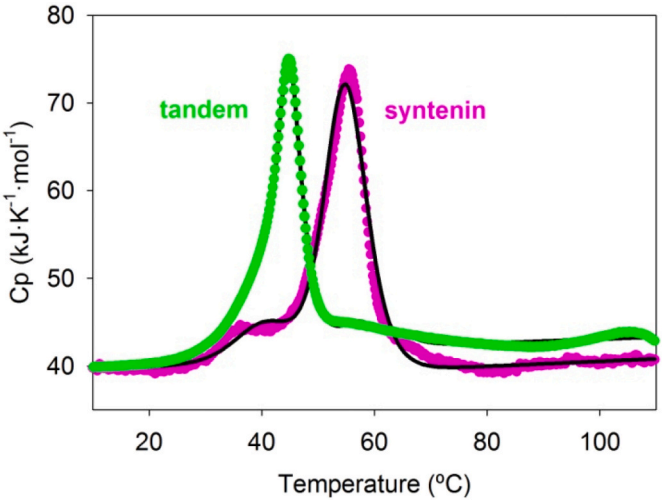

Fig. 2. Comparison between the DSC profiles of full-length Syntenin-1 (pink symbols) and the PDZ tandem (green symbols) under TP6 conditions at 10 μM and 100 μM concentration, respectively. The best fitting to the four-state model described by Scheme 2 is shown as a black line. For a better comparison, the DSC profile of the full-length protein has been moved down in the Cp axis to the position of the tandem.

not accompanied by a parallel reduction in the unfolding enthalpy, which can be estimated from the area below the heat capacity transition. This strongly suggests that the N- and C-terminal domains do not contribute significantly to the main cooperative unit of Syntenin-1, which seems to be mostly constituted by the tandem of PDZ domains. In summary, the contextual effects provided by residues 1–112 (N-terminal domain) and 274–298 (C-terminal domain) are not relevant for the unfolding cooperativity of the full-length protein.

The lack of X-ray structures for the full-length protein precludes a structural assessment of this point. The AlphaFold prediction for human Syntenin-1 (PDB code: AF_AFO00560F1) shows a high uncertainty for the structural prediction of these regions, but reflects some helical content at the N-terminal domain. In any case, the AlphaFold model does not reveal specific interactions between the N- and C-terminal regions and the central PDZ tandem. The C-terminal region comprises only 25 amino acids, which might not be long enough to induce any structural arrangement. The N-terminal region, containing 112 amino acids, has been described to play an auto-inhibitory role, possibly regulated by Tyr phosphorylation, but nothing is known on its possible structure

[16]. Previous NMR studies, comparing the ^{1}H-^{15}N HSQC NMR spectra of two tandem constructs including the N- and C-terminal regions of Syntenin-1 respectively, as well as that of complete Syntenin-1, revealed that the N-terminal region is most likely unstructured and does not seem to interfere with the PDZ tandem, while the C-terminal region provokes a broadening of a number of signals, indicating an increased propensity to aggregation. In any case, these studies are not conclusive and reveal that these regions, mainly the C-terminal region, might retain some structure and probably develop some defined interactions with the PDZ tandem [17]. Despite this evidence, the higher CD-ellipticity observed for full-length Syntenin-1 compared to the isolated PDZ tandem is not accompanied by additional negative ellipticity at the 222 nm region (Fig. 1), which strongly suggests that under all the experimental conditions in this work the N- and C-terminal flanking regions are essentially unstructured.

2.3. Differential scanning calorimetry of the PDZ tandem of human Syntenin-1

Focussing in the Syntenin-1 PDZ tandem, a more exhaustive DSC study under different buffer conditions (TP2 to TP6) was undertaken. The results are shown in Fig. 3, where the best experiments obtained at three different protein concentrations have been collected: 100 μM, 50 μM and 25 μM. These experiments reveal interesting effects associated to the thermal unfolding of Syntenin-1 PDZ tandem. First, the unfolding main transition does not have the typical symmetrical shape of two-state behaviour, being clearly asymmetric. Second, noticeable protein concentration effects are observed, so that higher protein concentrations

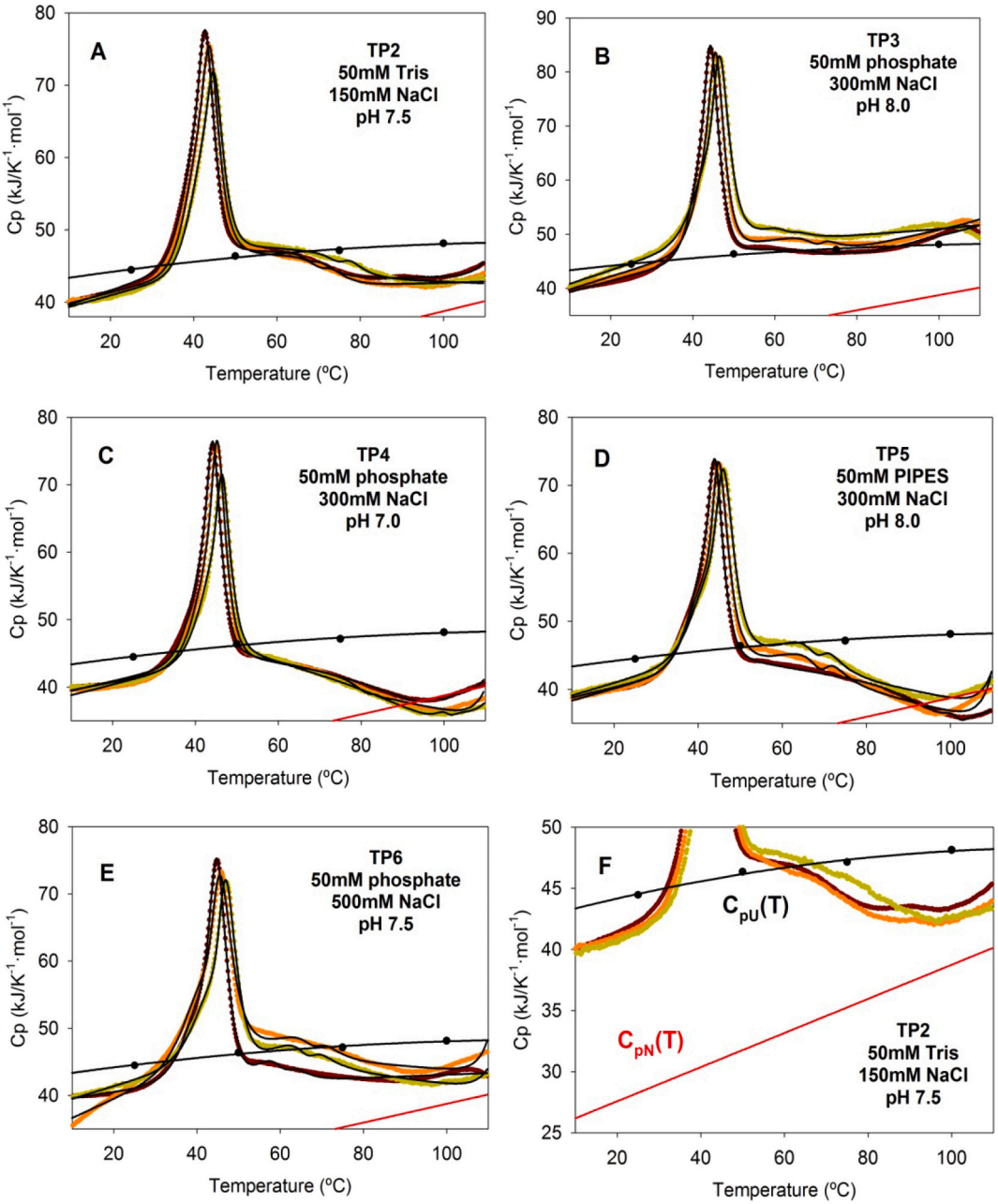

Fig. 3. The DSC unfolding traces of the PDZ tandem of Syntenin-1 under several buffer conditions. The experiments were carried out at three different protein concentrations: 100 μM (brown symbols), 50 μM (orange symbols) and 25 μM (green symbols). The black solid lines represent the best fit to the four-state model described in the text (Scheme 2). The black dotted line represents the $C_{pU}(T)$ function estimated from the amino acid composition [30,31] and the red solid line is the $C_{pN}(T)$ function estimated from the protein molecular weight [37].

give rise to lower T_m values. DSF experiments at different concentrations reproduce the same trend (Table S1). This concentration dependence indicates that the conformational state achieved after the transition has a higher oligomerization state than the native state. Finally, the theoretical $C_{pU}(T)$ function estimated from the amino acid composition [30,31] and describing the behaviour of the unfolded state, strongly deviates from the experimentally measured values (see all panels of Fig. 3). This clearly indicates that the macrostate populated after the main thermal-unfolding transition is an unfolding intermediate, rather than the fully unfolded state.

The simplest model that can account for these observations is a three-state scheme in which the intermediate state oligomerizes:

$$N \rightleftarrows 1/n\ I_n \rightleftarrows U \qquad \text{(Scheme 1)}$$

where N is the native state, I_n corresponds to an oligomeric intermediate state with n stoichiometry, and U the unfolded state. This model was used to fit the experimental DSC traces (see Materials and methods for details). An example reflecting the quality of these fittings is shown in the upper panel of Fig. S3, where it can be observed that, although the model reproduces well the main transition, it does not describe properly the post-transition heat effects occurring at high temperatures. The fitting quality at high temperatures noticeably improves when a fourth monomeric intermediate, I-state, is introduced in the scheme:

$$\begin{array}{c} N \rightleftarrows I \rightleftarrows U \\ \uparrow\downarrow \\ 1/n\,I_n \end{array} \qquad \text{(Scheme 2)}$$

Thus, this four-state model has been used to fit all the DSC traces obtained for the PDZ tandem construct (Fig. 3). Interestingly, the DSC profile obtained for full-length Syntenin-1 is also well reproduced by this four-state model (Fig. 2), but the resulting thermodynamic parameters are unreliable due to the irreversibility of the transition.

The thermodynamic formulation of the four-state model (Scheme 2) requires the optimization of several parameters through non-linear fitting: eight to describe the linear heat-capacity functions of the four macrostates ($C_{pN}(T)$, $C_{pI}(T)$, $C_{pIn}(T)$ and $C_{pU}(T)$), and six corresponding to the T_m values and the enthalpy changes of each of the three equilibriums. These results have been summarized in Table 1. The stoichiometry of the oligomeric intermediate, n, can be estimated from the protein concentration behaviour of these DSC traces as an additional fitting parameter. The best fits of the experimental data rendered a value of $n = 3$ for the intermediate stoichiometry, in agreement with previous studies performed with other PDZ domains [32]. Thus, $n = 3$ was used in any subsequent fittings.

In Fig. 4 the populations resulting from the thermodynamic analysis under TP2 conditions are shown. Similar distributions were obtained for the other conditions. The inspection of these results reveals that the monomeric intermediate may reach populations up to 30 % at temperatures above 40 °C, which justifies its inclusion into the model.

There exists a good consistency among the parameters derived from the fitting to the four-state model. Considering association/dissociation phenomena, the association processes should be exothermic and the dissociation ones endothermic. Accordingly, it can be observed (Table 1) that the enthalpy change, $\Delta H_{I\text{-}In}$, corresponding to the association of the intermediate is negative, whereas the other equilibriums give rise to positive enthalpy values. A further inspection of the unfolding equilibrium (Table 1 and Figs. 3 and 4) shows that the main endotherm is mainly due to endothermic contributions whereas the post-transition heat-capacity effects result from a partial compensation of relatively high endothermic and exothermic contributions.

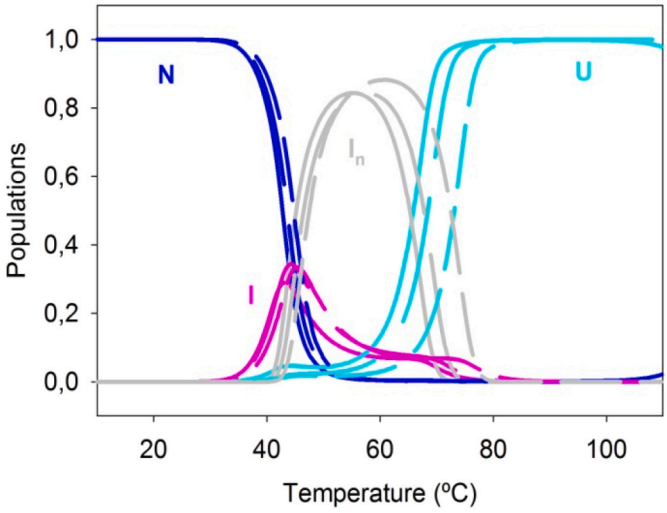

Fig. 4. Population analysis of the Syntenin-1 PDZ tandem in TP2 conditions, showing the temperature dependence of the population of the N-state (dark blue), the I-state (magenta), the I_n-state (grey), and the U-state (cyan). Continuous lines correspond to the populations at 100 μM protein concentration, long-dashed lines at 50 μM, and short-dashed lines at 25 μM.

In addition, the single transition obtained from CD and DSF experiments (Figs. S1 and S2) coincides with the main DSC endotherm (Fig. 3), mostly associated to the N ⇄ I heat contribution, which indicates that the structural transition corresponds to this equilibrium. The absence of any other structural evolution by CD and DSF upon temperature, together with the absence of residual ellipticity after the transition, indicate that the intermediates lack any defined secondary or tertiary structure, being thus structurally close to the unfolded state. Similar conclusions were obtained by our team from the unfolding analysis of other PDZ domains [32] and other proteins displaying this kind of oligomeric intermediates [4]. These results show that, although there is no true structural transition in the equilibriums I ⇄ I_n and I ⇄ U, they have associated a relevant heat exchange arising from the association/dissociation of these macrostates. Our most recent mutagenesis studies on PDZ domains strongly suggest that these associations are mainly

Table 1
Thermodynamic parameters resulting from the fitting of the DSC traces of human Syntenin-1 PDZ tandem to a four-state unfolding model (Scheme 2)[a].

Solvent[b]	$T_{N\text{-}I}$ (K)	$\Delta H_{N\text{-}I}$ (kJ·mol^{-1})	$T_{I\text{-}U}$ (K)	$\Delta H_{I\text{-}U}$ (kJ·mol^{-1})	$T_{I\text{-}In}$ (K)	$\Delta H_{I\text{-}In}$ (kJ·mol^{-1})
TP2	318.3 ± 0.3	265 ± 4	334.0 ± 1.1	205 ± 9	361.5 ± 2.6	−216 ± 9
TP3	320.3 ± 0.5	276 ± 13	332.7 ± 0.8	175 ± 4	357.7 ± 0.8	−260 ± 10
TP4	321.9 ± 0.5	253 ± 8	322.1 ± 1.6	10 ± 10	383,1 ± 4.0	−316 ± 7
TP5	319.8 ± 0.5	206 ± 5	332.1 ± 0.3	190 ± 6	360.6 ± 0.6	−181 ± 26
TP6	321.8 ± 1.0	173 ± 17	321.0 ± 3.3	72 ± 32	364.5 ± 4.4	−194 ± 39
Erbin-PDZ[c]	336.8 ± 0.2	382.0 ± 1.6	390 ± 5	165 ± 6	399.0 ± 3.4	−60 ± 8
PSD95-PDZ2[c]	334.4 ± 0.2	351.0 ± 0.3	312 ± 2	157 ± 2	408.5 ± 0.4	−153 ± 2

[a] The values represent the average of the six experiments. The intervals reflect the standard error of the average.
[b] TP2 (50 mM Tris, 150 mM sodium chloride, pH 7.5); TP3 (50 mM sodium phosphate, 300 mM sodium chloride, pH 8.0); TP4 (50 mM sodium phosphate, 300 mM sodium chloride, pH 7.0); TP5 (50 mM PIPES, 300 mM sodium chloride, pH 8.0); TP6 (50 mM sodium phosphate, 500 mM sodium chloride, pH 7.5).
[c] Extracted from [36].

based on hydrophobic interactions [33–35].

It is interesting to point out that PDZ domains seem to follow a similar unfolding mechanism involving the association of partially unfolded intermediates. In this way, the same model used to fit the DSC traces of the Syntenin-1 PDZ tandem (Fig. 3) describes well the unfolding equilibrium of other isolated PDZ domains from several proteins, including Erbin-PDZ and PSD95-PDZ2 [36]. The experimental DSC endotherms measured of the isolated Erbin and PSD95 PDZ domains are comparable to those of the Syntenin-1 tandem (Fig. 5), with the later showing unfolding enthalpies slightly smaller than those of the isolated PDZ domains from Erbin and PSD95 proteins (Table 1). The DSC analysis renders a stability for the Syntenin-1 PDZ tandem in the range of 20 to 30 kJ·mol^{-1}, a value that is small for a 21 kDa protein.

Comparison of the theoretical native and unfolded heat capacity functions (derived from well-ordered globular proteins and calculated from the molecular weight [37] and the amino acid composition [30,31] of the protein respectively) and the experimental values (Fig. 3F) informs on the degree of structuring of the N and U states of the protein. The experimental post-transition heat effects preclude the comparison between the experimental and theoretical $C_{pU}(T)$ functions. Nevertheless, there is a remarkable divergence between the experimental and theoretical native state heat capacity functions, $C_{pN}(T)$, so that the measured native state heat capacity is well above the estimated function. Since these constructs do not have long N- or C-terminal tails nor large loops that may be unstructured, this is indicative of a higher than expected flexibility of the native protein as a whole ([4,38] and references therein), and is in agreement with the low unfolding enthalpy and stability found for the tandem construct.

2.4. Differential scanning calorimetry of the PDZ1 and PDZ2 isolated domains

To gain further insight into the conformational behaviour of the tandem construct and to understand the origin of its low structural stability, the thermal unfolding equilibrium of the two isolated PDZ domains was studied. DSC experiments at different domain concentrations under TP6 conditions were performed (Fig. 6). These results show that, even under conditions of maximum stability, the unfolding cooperativity of the two isolated domains is poor: the height of the DSC traces is 10–15 kJ·K^{-1}·mol^{-1}, much smaller than the 40 kJ·K^{-1}·mol^{-1} usually found for other PDZ domains (Erbin-PDZ and PSD95-PDZ2) and also for the Syntenin-1-PDZ tandem (Fig. 5).

The DSC profiles for the isolated Syntenin-1 PDZ domains could be fitted to the four-state model (Scheme 2). However, using such a complex model is not justified in this case, since the fitting quality was not significantly improved with respect to three-state model (Scheme 1). The thermodynamic parameters derived from the simpler three-state model have been summarized in Table 2. The unfolding parameters for the isolated PDZ domains are small compared to those typically found for standard proteins of similar size. In this way, the unfolding enthalpies are much smaller than those of Erbin-PDZ and PSD95-PDZ2 (Table 1), and comparable to those of SH3 domains, which are much smaller in size (7 kDa; [39]). A similar situation is found for the changes in Gibbs energy (stability). In addition, the association heats for the Syntenin-1-PDZ2 domain are smaller than those obtained for the Erbin-PDZ and PSD95-PDZ2 domains, being almost negligible for Syntenin-1-PDZ1. Finally, while the different techniques (DSC, CD and DSF) rendered very similar T_m values for the tandem construct, a divergence of approximately 5 °C was found between the different techniques for the isolated PDZ domains.

In summary, the poor cooperativity displayed by the unfolding transitions of the isolated PDZ domains is reflected in a low reproducibility of the traces, which introduces a great uncertainty in the determination of the thermodynamic parameters. Thus, although the quality of the fitting is good (Fig. 6), the numerical results may not have sufficient reliability. Supporting these conclusions, the temperature dependency of the population of the three states for each isolated Syntenin-1 PDZ domain, shown in Fig. S4, reveals a great and not usual scattering in the population distributions at high temperatures, confirming the poor quality of these DSC experiments.

These results indicate that, in the tandem configuration, the two PDZ domains establish interactions leading to a notable increase in cooperativity, as illustrated in Fig. 7, where the relative magnitudes of the DSC unfolding transitions for the isolated PDZ domains and the tandem are compared. The experimental trace for the PDZ tandem reveals an increase in cooperativity with respect to the sum of the individual domain

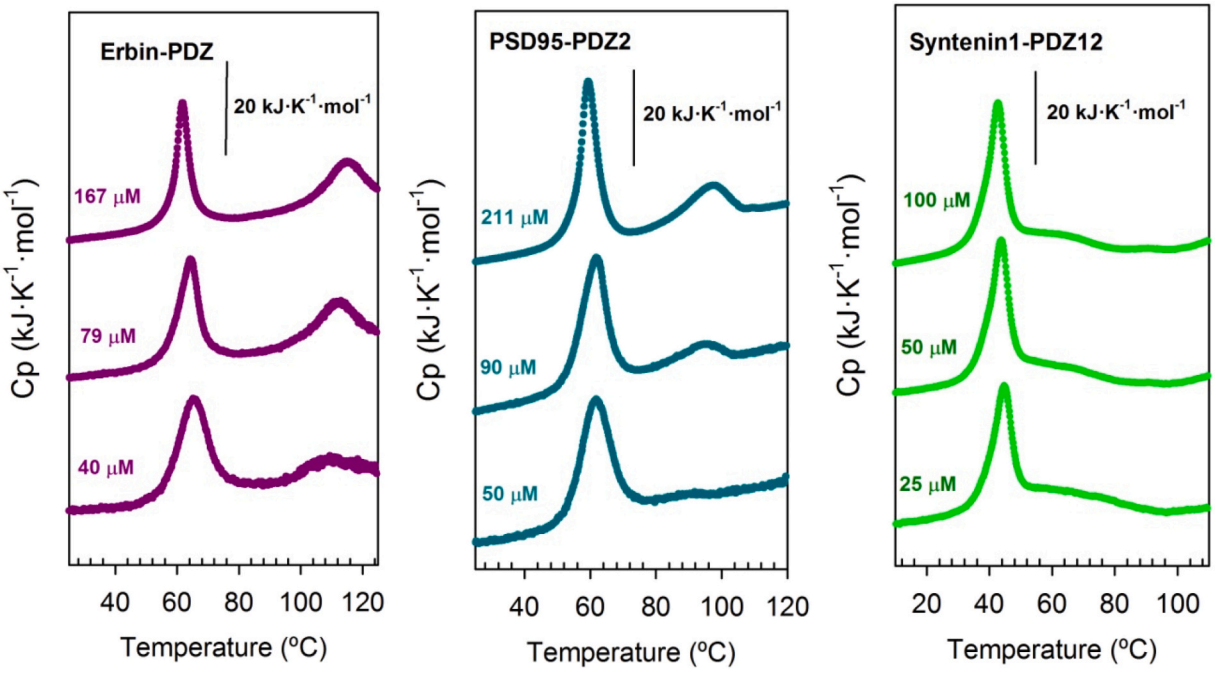

Fig. 5. Comparison between the DSC traces at different protein concentrations of Erbin-PDZ (purple symbols) and PSD95-PDZ3 (cyan symbols) isolated domains, and the PDZ tandem of human Syntenin-1 (green symbols). The experiments with the isolated PDZ domains have been published previously [36].

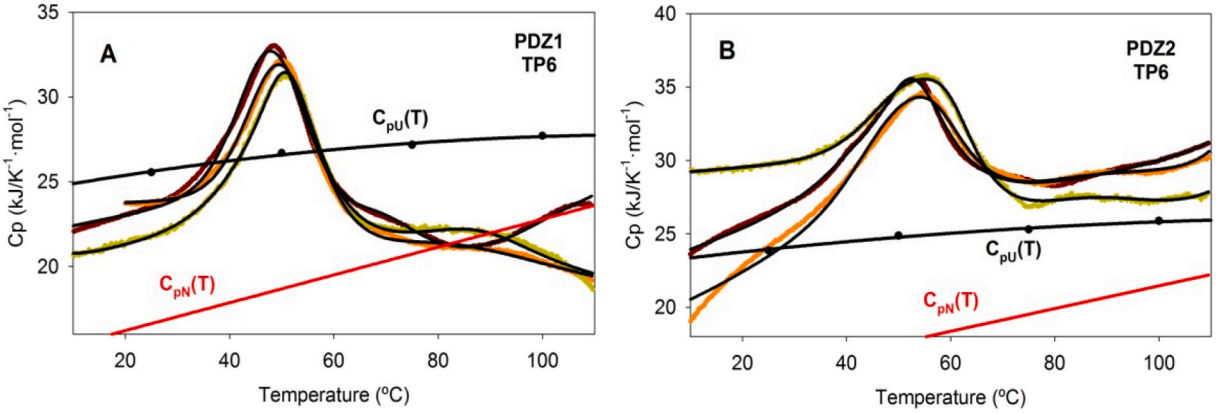

Fig. 6. DSC unfolding profiles for the isolated PDZ1 **(A)** and PDZ2 **(B)** domains of Syntenin-1 under TP6 buffer conditions. The experiments were carried out at three different protein concentrations: 100 μM (brown symbols), 50 μM (orange symbols) and 25 μM (green symbols). The black solid lines represent the best fit to the three-state model described in the text (Scheme 1). The black dotted line represents the $C_{pU}(T)$ function estimated from the amino acid composition [30,31] and the red solid line the $C_{pN}(T)$ function estimated from the protein molecular weight [37].

Table 2
Unfolding thermodynamic parameters derived from the fitting to a three-state denaturation model (Scheme 1) of the DSC profiles of isolated Syntenin-1 PDZ1 and PDZ2 domains[a].

Domain	T_{N-U} (K)	ΔH_{N-U} (kJ·mol^{-1})	T_{I-In} (K)	ΔH_{I-In} (kJ·mol^{-1})	$\Delta G_{N-U}(298)$ (kJ·mol^{-1})
PDZ1	324 ± 2	165 ± 15	365 ± 15	−25 ± 25	8 ± 3
PDZ2	326 ± 2	130 ± 10	380 ± 5	−35 ± 5	9 ± 2

[a] The values represent the average of the three experiments performed at different protein concentrations under TP6 solvent condition. The intervals reflect the standard error of the average.

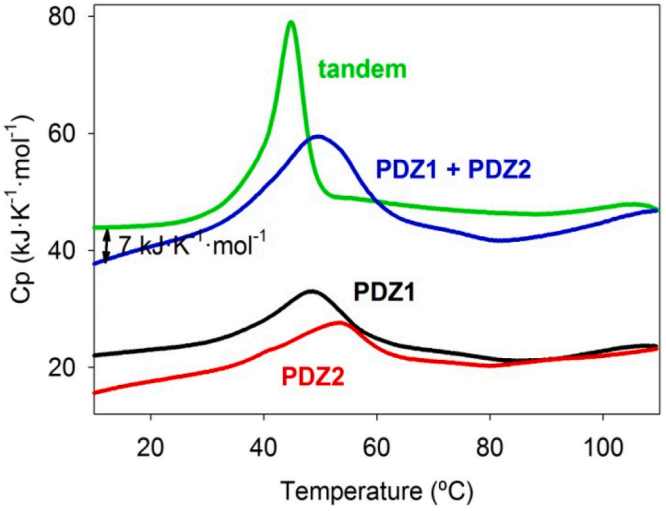

Fig. 7. Comparison of the DSC profiles of the two isolated PDZ domains of human Syntenin-1, PDZ1 (black line) and PDZ2 (red line), and the PDZ tandem (green line). The blue line is the sum of the transitions corresponding to the isolated PDZ1 and PDZ2 domains. In all cases, protein concentration was 100 μM.

contributions, accompanied by a decrease of the T_m value, indicating strong interactions between the two PDZ domains. These results, together with previous NMR-titration experiments that discard the direct interaction between the individual domains in solution, suggest that the linker sequence plays an important role facilitating the interactions between the two PDZ domains in the tandem configuration [17].

2.5. Structural analysis of the Syntenin-1 PDZ tandem interface

To gain additional insight into the origin of the cooperativity between Syntenin-1 PDZ domains, the ten high resolution structures of the Syntenin-1 PDZ tandem deposited at the Protein Data Bank were analyzed. The unbound structure (PDB entry: 1n99) and all the complex structures available up to date (PDB entries: 1obz, 1v1t, 1w9e, 1w9o, 1w9q, 1ybo, 4z33, 6r9h, 6rlc) [40–42], which include different ligands bound to the PDZ1 or PDZ2 domain, were considered for the analysis. All tandem structures were obtained with the same construct (sequence and length) used in this study (residues 113–273, corresponding to the PDZ1 domain: Arg113-Arg193, and the PDZ2 domain: Arg197-Phe273, joined by a short Pro194-Phe195-Glu196 linker). Even though PDZ1 and PDZ2 domains have <30 % identity in their amino acid sequence, the superposition of the backbone atoms results in a low *rmsd* value (1.1 Å), which points to a very conserved structural fold. Besides the C-terminus whose four-five last residues are unstructured, the most significant differences are located at the β2-β3 loop, which is shorter in PDZ2, and in the binding site cleft, which is narrower in PDZ1 compared to PDZ2 and other PDZ domains. The structural difference in the binding site region has been proposed to account for the lower binding affinity shown by Syntenin-1-PDZ1 for its ligands [40].

It has been described elsewhere that both PDZ domains have different specificity profiles; in addition, some studies indicate that the two domains can work cooperatively, giving rise to higher affinities for the protein targets when the two domains are in tandem [41]. The superposition of the backbone atoms of the complex structures of the PDZ tandem, using the unbound structure coordinates as a reference (chain A of the PDB entry 1n99), gives low *rmsd* values (Table S2). This strongly suggests that both domains interact to keep their mutual arrangement. Supporting this assumption, NMR residual dipolar couplings measurements reveal that the disposition of the PDZ domains in X-ray structures is retained in solution [17].

Inspection of the unbound structure of the PDZ tandem reveals a cluster of salt-bridged residues composed of Arg153 and Arg193 from PDZ1, Glu196 from the linker, and Glu240 from the PDZ2 (Fig. 8A). This cluster is also present in the complex structures, which, in some cases, show alternate conformations of these side chains and the presence of some water molecules mediating these interactions (Fig. 8B). In addition to these electrostatic interactions some hydrophobic contacts are observed. In this way, Phe154 from PDZ1 is packed between the aliphatic chains of Ile247 and Met270 from PDZ2 (Fig. 8C). Also, Pro194, the first residue of the short linker, is expected to restrict the conformational space of both domains. This proline residue is located next to Arg193, which appears in an unfavourable region of the

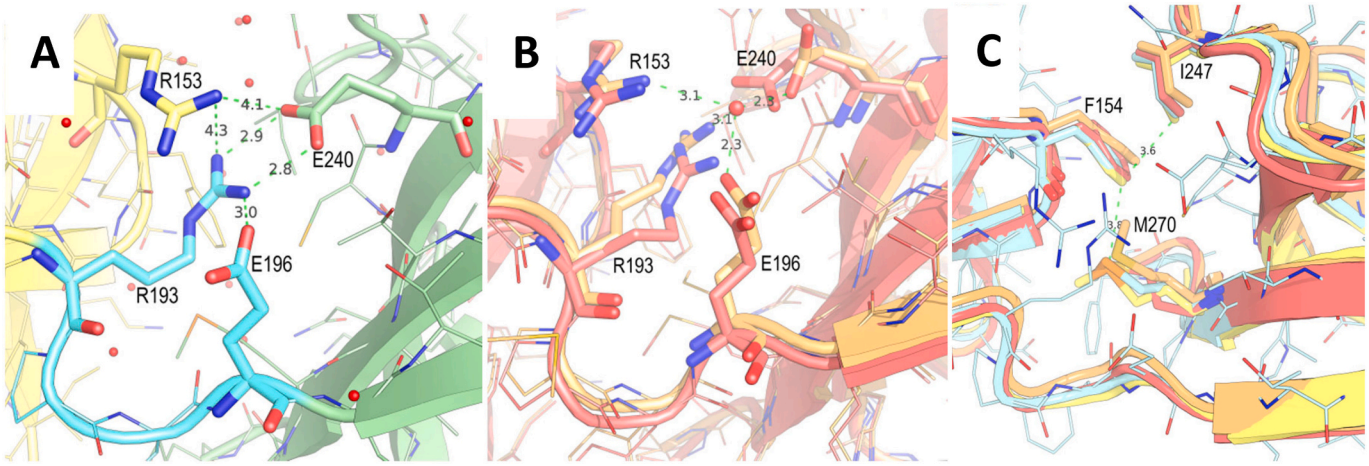

Fig. 8. **(A)** Electrostatic interactions at the PDZ1/PDZ2 interface of free Syntenin-1 PDZ tandem structure (PDB entry 1n99) and of its complex with the TNEFYF peptide (PDB entry 1w9e) structures. The residues implicated in salt bridge formation are shown as sticks. For sake of clarity only the chain-A structure of the unbound tandem (PDB entry 1n99) is shown, where the PDZ1 (yellow), the linker (cyan) and the PDZ2 (green) are shown in cartoon representation, and the relevant side chains as sticks. **(B)** Superposition of the chains A (orange) and B (salmon) of the bound structure (PDB entry 1w9e). Electrostatic interactions are mediated by a water molecule (red sphere) in chain A. Chain B shows the interaction pattern observed for the unbound structure. **(C)** Hydrophobic interactions in the PDZ1/PDZ2 interface of the unbound Syntenin-1 PDZ tandem (PDB entry 1n99, chain A cyan and chain B yellow) and of its complex with the TNEFYF peptide (PDB entry 1w9e, chain A orange and chain B salmon). Residues Phe154, Met270 and Ile247 are shown as sticks. Distances between these residues are shown as dash green lines. For the sake of clarity only the side chains of the unbound chain A are shown as sticks.

Ramachandran in most of the tandem structures (*i.e.* 1n99 and 1w9e). The high energy of the conformation adopted by the linker seems to be offset by the interactions established at the interface of the PDZ domains.

Occluded water molecules were consistently found at the PDZ1/PDZ2 interface in the different tandem structures, mediating the interactions between the two domains. Up to nine conserved hydration sites organized in two main clusters (Fig. 9) were systematically observed in the different crystal structures. The first hydration cluster (positions W1 to W3) is coordinated by residues from the PDZ1 domain. Waters at W1 are fully buried and hydrogen bonded to the backbone atoms of residues Gly155 and Phe195. The second hydration cluster (sites W4 to W9) is located next to Arg193 and Glu240, and close to Phe154, Ile247 and Met270 participating in hydrophobic interactions between both domains (Fig. 8C). Water molecules around the hydrophobic residues (W1–W2 and W4–W6) are fully buried (ASA values <15

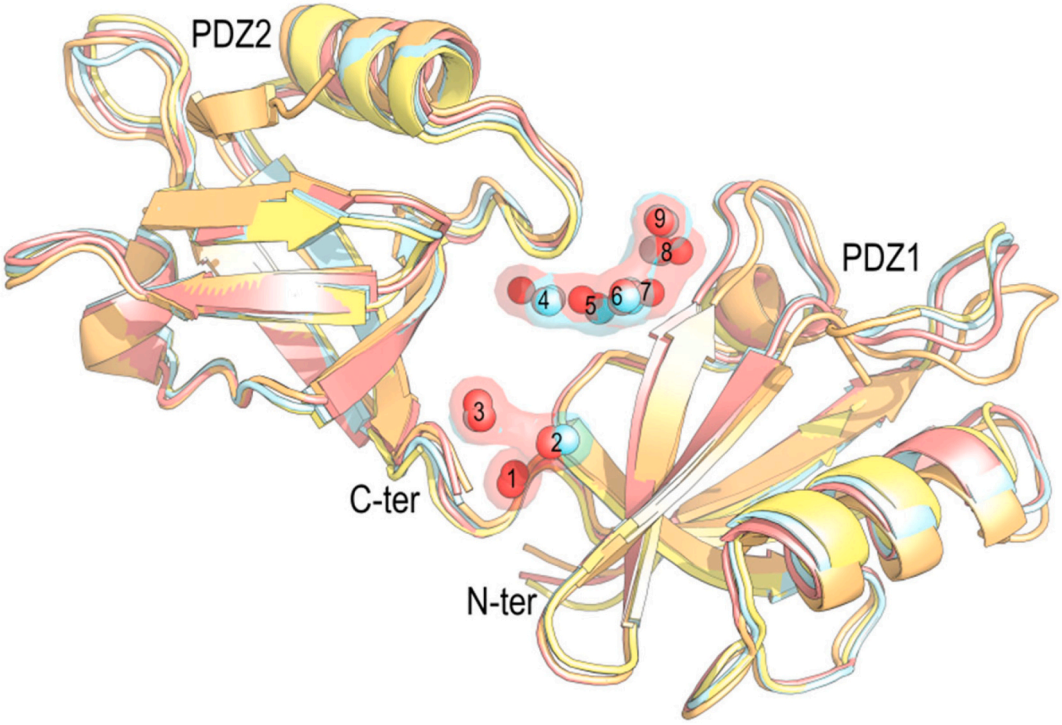

Fig. 9. Hydration spots at the PDZ1/PDZ2 interface of the Syntenin-1 PDZ tandem. Conserved water molecules are shown as spheres, those from the unbound structure are coloured in cyan and those from the peptide bound structure are coloured in red. The numbers used to identify the waters in the figure are those shown in Table 3. The interface between PDZ1 and PDZ2 domains in the tandem construct of the unbound (PDB entry 1n99, chain A cyan and chain B yellow) and of the bound with TNEFYF peptide (PDB entry 1w9e, chain A orange and chain B salmon) structures are shown in a cartoon representation.

Å^2) and characterized by B-factor values similar to the surrounding protein residues (Table 3).

3. Discussion

The initial goal of this work was the energetic and structural analysis of Syntenin-1 unfolding, a multi-modular protein containing a tandem of two PDZ domains in its central region flanked by two different domains at the N- and C-terminus. The poor solubility of the protein, the irreversibility of the unfolding transition, and, possibly the coupling of a homo-oligomerization equilibrium mediated by the C-terminal domain, have precluded a thorough thermodynamic analysis of the unfolding equilibrium for full-length Syntenin-1. Nonetheless, our experiments reveal that the flanking N- and C-terminal domains do not seem to contribute significantly to the cooperative unit of this protein, since the tandem of PDZ domains (residues 113–273) accounts for >90 % of the unfolding enthalpy (which can be easily estimated from the area under the heat capacity curve in the DSC experiments) (Fig. 2). This tandem displays a much higher solubility, a partly reversible unfolding transition (>50 %), and is monomeric under the experimental conditions used in this work.

The thermodynamic behaviour of the PDZ-tandem unfolding is characterized by relatively low cooperativity, comparable to that of archetypical PDZ domains (Fig. 5 and Table 1), but still unusually high when compared to the expected contribution of the isolated domains (Fig. 7). This gain in cooperativity of the tandem translates into a high value for the unfolding enthalpy. Nevertheless, the stability values, $\Delta G_{N\text{-}U}(298)$, are in the range 20–30 kJ·mol^{-1}, small for a 21 kDa protein and compatible with the relatively low cooperativity displayed upon unfolding.

Analysis of the interface between the PDZ domains in the crystallographic structures available for the tandem construct reveals a set of conserved interactions, some of which are mediated by water molecules. These waters are buried from the solvent and display B-factors comparable with those of the surrounding protein residues (Table 3), which guarantees a high occupancy of the hydration spots in solution [43–45]. Two main hydration clusters have been identified, interconnecting polar side chains at the interface between the two PDZ domains (Fig. 9). The hydrophobic environment provided by Phe154, Ile247 and Met270 side chains increases the energy of these electrostatic interactions.

Table 3
B-factors and ASA values for the occluded water molecules at the PDZ1/PDZ2 interface in human Syntenin-1 tandem structures.

PDB	1n99		1w9e	
Resolution (Å)	1,94		1,56	
Chain[a]	A	B	A	B
B-factor average (Å^2)	27	26	23	24
Water number	Residue number/B-factor (Å^2)/ASA (Å^2)			
W1	312/33.6/0	401/50.0/0	2067/19.2/1.90	2044/21.41/0.00
W2	396/41.1/2.90	388/35.7/3.70	2066/44.1/7.50	2025/45.08/4.00
W3	316/42.54/4.80	–	215/37.7/46.20	2173/30.3/3.40
W4	287/29.29/6.60	307/35.46/4.40	2166/58.13/2.80	2152/29.1/3.20
W5	291/23.78/9.60	297/32.5/10.10	2124/32.1/13.30	2042/24.8/8.10
W6	294/26.80/3.80	311/33.7/3.20	2065/25.4/18.60	2030/31.5/4.00
W7	354/42.06/28.60	315/52.8/26.10	2061/37.1/36.30	2041/37.3/24.10
W8	327/44.48/29.80	361/46.9/28.50	2052/37.0/45.80	2028/44.0/29.20
W9	310/47.06/31.60	372/41.1/29.30	–	2029/42.5/25.30

[a] The structures of the unbound PDZ tandem (1n99) and the complex structure (1w9e) have two chains in the asymmetric unit. The analysis of both chains is shown.

The immediate thermodynamic consequence of embedded waters upon protein unfolding would be a strong enthalpy−entropy compensation. These effects have been revealed by us in previous unfolding studies with the CD2BP2-GYF domain [46]. This small protein domain unfolds as a two-state protein, showing a stability according to its size but a higher than usual unfolding enthalpy. The structural analysis of its single cooperative unit revealed several cavities and pockets into the hydrophobic nucleus of this domain, able to be occupied by water molecules. These occluded waters may thus explain the large unfolding enthalpy found in CD2BP2-GYF because the extra-amount of hydrogen bonds that can be established in the N-state, up to four by each water molecule, as well as the extra-entropic contribution by desolvation upon unfolding [47].

Overall, hydration increases the flexibility of the protein ([47,48] and references therein). This feature can be easily evaluated from DSC experiments as it is reflected in the increase of the experimental $C_{pN}(T)$ function with respect to the standard values estimated from the protein molecular weight [4,37,38,49]. In the case of Syntenin-1 PDZ tandem, there is a difference of 7 kJ·K^{-1}·mol^{-1} between the $C_{pN}(T)$ function corresponding to the experimental DSC trace of the tandem and the values obtained by the sum of the isolated PDZ1 and PDZ2 DSC profiles (Fig. 7). Such a difference may well be attributed to the waters at the interface. In this context, a part of the whole entropy change would result in an increase in conformational freedom because the hydrogen bonds between protein atoms at the interface get longer by the intercalated waters, which might contribute to the increase in flexibility. The effect could be as if water acts as a lubricant into protein packing [47]. Oppositely, there exists an entropic loss coming from the immobilization of the water molecules at the interface but, from an energetic point of view, these bound waters increase the vibrational entropy of the protein [50]. Molecular dynamics studies have revealed that these fluctuations arise when water molecules get away or go in the protein interface. These features have been seen both inside the proteins [51] and upon ligand binding [44].

An interesting energetic effect of waters is that the dynamics of water inside the protein core will also affect protein thermostability. Water content has been established as a relevant criterion to distinguish between mesophilic and psychrophilic (cold-adapted) protein homologues, the latter containing a larger number of water molecules occluded within the structure [48]. In fact, in the case of CD2BP2-GYF the T_m values are lower (among 40 − 55 °C; Table 1) than the averaged 60 °C obtained by Robertson and Murphy from a big data set built with the unfolding data of globular proteins [52], or even than the ones of other proline-binding domains [38,39,49]. The low thermostability was closely related in the CD2BP2-GYF domain to the high ΔCp_{N-U} value (8.4 kJ·K^{-1}·mol^{-1}), responsible for the strong curvature of the Gibbs energy function that narrows the stability interval of the domain [46]. In the case of the Syntenin-1 PDZ tandem a T_m value of 45 °C is observed, lower than the obtained for the isolated PDZ domains, as well as the acquired from the addition of the DSC traces of both PDZ domains (Fig. 7).

It can be hypothesized that the inclusion of these hydration regions between the domains may well have a similar effect to the previously observed for CD2BP2-GYF. In this way, the four-state model used to fit the DSC traces of the tandem (Fig. 3) has been previously used to describe the unfolding of isolated PDZ domains, such as Erbin-PDZ and PSD95-PDZ2 [36]. These observations strongly support the idea that the electrostatic and hydrophobic interactions, together with the observed structural water molecules found at the interface of Syntenin-1 PDZ tandem, contribute to generate a full cooperative unit between both PDZ domains, and that this unit retains the more salient features displayed by PDZ domains upon unfolding. Supporting these conclusions, the unfolding enthalpies of the tandem are smaller than those of Erbin-PDZ and PSD95-PDZ2 isolated domains ($\Delta H_{N\text{-}I}$ and $\Delta H_{I\text{-}U}$ values in Table 1)

and, therefore, they are smaller than the expected enthalpy changes for a tandem of two PDZ domains, despite the positive contribution of the interfacial water molecules. This fact is a consequence of the scarce contribution of both PDZ domains due to their poor unfolding cooperativity. Nevertheless, the association enthalpy of the tandem intermediate ($\Delta H_{I\text{-}In}$) is higher, almost double, than the respective of the archetypical Erbin-PDZ and PSD95-PDZ2 domains, because each tandem molecule possess two unfolded domains associating more or less independently.

Inspection of the few existing PDZ-tandem structures available at the PDB reveals different scenarios in which PDZ domains cooperate within a tandem configuration, modifying its binding properties with respect to the isolated domains. Some examples demonstrate that the tandem is stabilized by interactions established between the C-terminus of the second PDZ domain and any region of the first one. This is the case of GRIP1-PDZ45 [53,54] and INAD-PDZ45 [55] arrays. Recent biophysical studies on the X11-PDZ12 tandem [8] showed that the binding of its PDZ2 C-terminal tail to the PDZ1 binding site is critical to ensure the cooperative folding of the tandem [56]. Thus, in these cases, long-range interactions seem to justify cooperativity, with the interfaces not being energetically relevant. The low resolution of the X-ray structures and the lack of this information in the NMR ensembles preclude a thorough revision of the buried waters molecules at the interfaces in these PDZ repeats. The only tandem structure at enough resolution to reliably evaluate the presence of interfacial waters is the one of the PDZ tandem of GRASP domain (PDB code: 3rle; resolution at 1.65 Å), where an internal sequence of PDZ2 packs against the PDZ1 binding pocket [57]. Partially buried water molecules (ASA values <10 Å^2) were found at the PDZ1/PDZ2 interface (Fig. S5) resembling the hydration pattern found for the Syntenin-1 tandem.

In the case of GRIP1-PDZ12 tandem the binding pocket of PDZ2 is occluded when it interacts with the PDZ1 domain, but there are no interactions outside the interface [58]. This scaffolding behaviour of one of the PDZ domains on the other would not be the case of the Syntenin-1 tandem, where both domains have been described as functional. Interestingly, the GRIP1-PDZ12 X-ray structure (PDB code: 2qt5) confirms the presence of some water molecules fully buried at the interface (ASA $= 0$ Å^2) which may have a similar energetic role to those described in the Syntenin-1 tandem (Fig. S5), since the disposition of these waters is roughly well reproduced in the two chains of the structure. A similar "front-to-back" arrangement to Syntenin-1 has been observed in the supramodule established by the Scribble-PDZ45 tandem. The unbound (PDB code: 4wyt) and the bound (PDB code: 4wyu) structures do not reveal the presence of water molecules at the interface, due to the low resolution of the structures (2.5 Å) [59].

Other examples reporting non-cooperative tandem arrangements can be found in the literature. Among them, the PDZ12 tandem of PSD95 protein has been studied deeply. It is characterized by a mutual disposition between the PDZ domains that allow both active sites to be operative, being the isolated domains stable and equally functional in solution [60,61]. The different structures (PDB codes: 2KA9, 3GSL, 3ZRT) show no relevant interfaces between the structural models. Molecular dynamics simulations confirm that the relative orientation of the two domains covers a large conformational space, where ligand binding will restrict this conformational space to a more defined arrangement [62–64].

Extensive folding/unfolding studies with non-cooperative tandem repeats have been carried out with the Whirlin-PDZ12 tandem, where it has been described that a transient misfolding intermediate can interact with its physiological ligand. The net difference in stability between the two PDZ domains and the lack of additional cooperativity in the tandem arrangement makes this example ideal for studying the effect of contiguous domains on the folding of a tandem array. From the kinetic analysis of exhaustive mutational work on PDZ1 in the context of the tandem and in isolation, it could be concluded that the late events of folding of this tandem construct are robust. In contrast, the early events are much more diffuse and undergo clear conformational changes that compare well with the frustration patterns of the domain, suggesting that alternative pathways and protein misfolding may arise in multidomain folding proteins from locally non-optimized regions [9–11]. The same authors have described a very similar behaviour for the PDZD2-PDZ56 tandem. In this case, the misfolding intermediate displays even better binding affinity than the native state [12].

An interesting point that comes from these unfolding studies is the potential formation of swapped species in the folding/unfolding process of a PDZ-tandem. Thus, the competence between the functional unfolding intermediate and productive folding suggests that such a functional intermediate would have the PDZ domains in an intertwined fashion [9]. Since the equilibrium unfolding studies with Syntenin-1 constructs and with other isolated PDZ domains reveal an obligatory self-associating intermediate that populates at mid-temperatures upon unfolding, the question would be if these equilibrium and kinetic intermediates are conformationally related or not. The answer comes from previous extensive studies carried out with the isolated PSD95-PDZ3 domain, where structural information about the low-energy equilibrium intermediates has been obtained by NMR spectroscopy [36] and Φ-value analysis provided it for the high-energy folding transition state [65]. The comparison revealed compatible results, being the regions of α2 and β5 relatively well structured, whereas the central β-strands appear as mostly unstructured. This scenario is fully compatible with domain swapping, since the known examples in PDZ domains use to share the β2-β3 hairpin, which is included within the most unstructured region in these unfolding intermediates of PSD95-PDZ3. As we already stated in the Results, the most recent mutagenesis studies on PSD95-PDZ3 domain strongly suggest that self-assembling of these equilibrium intermediates is mainly due to hydrophobic interactions between specific residues located in such unstructured regions [33–35].

In summary, the few examples described to date on energetic and structural studies on PDZ-tandem arrangements expose a variety of possible situations. In this context, the fully cooperative behaviour of Syntenin-1-PDZ12 constitutes a new approach where both PDZ domains, already functional although unstable when isolated, can cooperate through a front-to-back attachment. This arrangement is favoured by some electrostatic and hydrophobic interactions, where several buried water molecules at the interface provide additional interactions between both domains. Similar interactions have been found in the structures of GRIP1-PDZ12 and GRASP-PDZ12. On the other side, a few examples where a fully cooperative arrangement has also been described have revealed long-range interactions between their C-terminus and any defined region at the first PDZ domain. The folding studies with truncated constructs of X11-PDZ12 have demonstrated that such interactions would be the main responsible of cooperativity in these cases. Thus, more PDZ-tandem arrays must be explored to discern whether the mechanism described here for Syntenin1-PDZ12 to achieve unfolding cooperativity might also be applied to other PDZ tandems.

4. Conclusions

The energetic analysis of the Syntenin-1 PDZ tandem presented here reveals that the interactions at the interface between the two PDZ domains are strong enough to generate a fully-cooperative structure with energetic features similar to those previously described for other isolated PDZ domains. The relatively low T_m values (45 °C), as well as the high heat capacity of the native state (above 40 kJ·K^{-1}·mol^{-1}) and unfolding enthalpy (higher than 400 kJ·mol^{-1} under some of the studied conditions) of the Syntenin-1 PDZ tandem are consistent with the presence of a set of conserved interfacial water molecules bridging interactions at the interface between its two PDZ domains in the crystal structures. Thus, the energetic relevance of these interfacial water molecules on these PDZ tandem constructs can be hypothesized and is something worth studying, which makes necessary to extend this type of studies to other cooperative PDZ tandem arrays.

5. Materials and methods

5.1. Protein expression and purification

The original sequences of human Syntenin-1, also known as SDCBP protein (residues 1–298; UniProtKB code O00560·SDCB1_HUMAN), the PDZ tandem (residues 113–273), and the isolated PDZ1 (residues 113–193) and PDZ2 (residues 197–273) domains, were optimized for expression into *Escherichia coli* BL21/DE3 (Novagen) and cloned into pETM11 plasmid (EMBL Core Purification Facility, Heidelberg, Germany) using *Nco*I and *Hin*dIII restriction sites. This work was carried out by the company Geneart (ThermoFisher Scientific). The different constructs, containing a 6xHis-tag at the N-terminus, were expressed in bacterial cultures, LB-Kanamycin medium, at 37 °C up to an optical density at 600 nm of approximately 0.6, when the temperature was lowered to 25 °C. Then, the cultures were induced with 0.5 mM IPTG and allowed to grow at 25 °C overnight. Bacterial pellets were resuspended in binding buffer (50 mM sodium phosphate, 500 mM NaCl at pH 7.5), and lysed by French press. The clarified lysate was bound in a 5 mL prepacked Ni-Sepharose column (Cytiva™). The column was washed twice with washing buffer (50 mM sodium phosphate, 500 mM NaCl, 20 mM imidazole at pH 7.5), and then the protein was eluted with elution buffer (50 mM sodium phosphate, 500 mM NaCl, 500 mM imidazole at pH 7.5). The ratio of highly pure protein per liter of LB culture obtained was: 20 mg for human Syntenin-1, 30 mg for its PDZ tandem, and 30 mg and 50 mg for the isolated PDZ1 and PDZ2 domains respectively. The purified proteins were frozen in liquid nitrogen and stored at -80 °C. The extinction coefficients were theoretically calculated in ProtParamExPASy server; the values at 280 nm were 15,930 $cm^{-1}{\cdot}M^{-1}$ for human Syntenin-1, and 8480 $cm^{-1}{\cdot}M^{-1}$ for the PDZ tandem and the PDZ1 domain. The extinction coefficient for the PDZ2 domain was 2800 $cm^{-1}{\cdot}M^{-1}$ determined in this case at 274 nm. Molecular masses of 35,571 Da (human Syntenin-1), 20,839 (PDZ tandem), 12,255 Da (PDZ1 domain) and 11,543 (PDZ2 domain) were obtained by MALDI-TOF experiments carried out at the Scientific Instrumentation Services (CIC) of the University of Granada. Experimental samples were always prepared by extensive dialysis against the corresponding buffer at 4 °C.

5.2. Differential scanning calorimetry (DSC)

Differential scanning calorimetry (DSC) experiments were carried out in an automated MicroCal VP-DSC instrument from Malvern Panalytical. DSC traces were generated at 1.5 $K{\cdot}min^{-1}$. The samples were routinely heated twice from 5 °C to 110 °C to check the reversibility of the unfolding process. Each experimental DSC thermogram was routinely corrected from the time response of the calorimeter and from the instrumental baseline. After normalization by protein concentration, the partial molar heat capacity curves were calculated from the resulting thermograms assuming 0.73 $mL{\cdot}g^{-1}$ for the partial specific volume and the respective molecular weight obtained from mass spectrometry. These calculations were made using ORIGIN software. Thus the baselines extracted from the analyses represent the net values for molar heat capacities and can be used as an additional criterion to justify the quality of our fitting analyses.

For the analysis of the DSC traces obtained at different protein concentrations it is assumed that a single set of thermodynamic magnitudes should be compatible with all the experimental traces, as it is considered by the model. Therefore, any differences in such thermodynamic magnitudes are consequence of the changes in equilibrium, solely induced by variations in protein concentration. The thermodynamic equations describing the three-state model shown in Scheme 1 have been described in detail in a previous work [32]. A total of 10 parameters can be optimized upon fitting, being $C_{pN}(T)$, $C_{pIn}(T)$ and $C_{pU}(T)$ linear functions for each experiment independently, as well as the $T_{N\text{-}U}$ and $T_{I\text{-}In}$, and $\Delta H_{N\text{-}U}(T_{N\text{-}U})$ and $\Delta H_{I\text{-}In}(T_{I\text{-}In})$ parameters related to the two equilibriums shown in Scheme 1. Otherwise, the four-state model described by Scheme 2 has been described elsewhere [66], displaying 14 fitting parameters. In this case, it was undertaken an overall analysis to obtain the heat-capacity $C_{pN}(T)$, $C_{pIn}(T)$, $C_{pI}(T)$ and $C_{pU}(T)$ linear functions for each experiment independently, as well as the $T_{N\text{-}I}$, $T_{I\text{-}In}$ and $T_{I\text{-}U}$, and $\Delta H_{N\text{-}I}(T_{N\text{-}I})$, $\Delta H_{I\text{-}In}(T_{I\text{-}In})$ and $\Delta H_{I\text{-}U}(T_{I\text{-}U})$ parameters related to the three equilibriums shown in Scheme 2. All fitting parameters were obtained individually for each experiment in an attempt to assess the realistic error associated to these values. Calculations were made using Sigma Plot 2000 (Systat Software Inc.).

5.3. Circular dichroism (CD)

CD measurements were taken in a Jasco J-715 spectropolarimeter equipped with a temperature-controlled cell holder. Far-UV CD spectra were recorded from 260 to 200–210 nm in 1 or 2 mm path length cuvettes. Each CD spectrum was obtained by averaging 4 accumulations collected at a scan rate of 50 $nm{\cdot}min^{-1}$. All spectra were corrected by buffer contributions and then normalized as mean residue molar ellipticity.

Temperature scans were conducted at a heating rate of 1.5 $K{\cdot}min^{-1}$ after equilibration of the measuring cell within the cell holder at 10 °C for 5 min. When the final temperature of 90 °C was reached, the samples were incubated for 5 min to record the spectrum of the unfolded state and then cooled down to 10 °C, at which point another spectrum was taken to check the reversibility of unfolding.

According to the two-state model (N ⇄ U) thermal denaturation experiments followed by CD were fitted individually to the following equation:

$$\Theta_{222}(T) = \frac{\Theta_{222,N} + \left(K_{N-U}{\cdot}\Theta_{222,U}\right)}{1 + K_{N-U}} \quad (1)$$

where $K_{N\text{-}U}$ is the equilibrium constant and $\Theta_{222,N}$ and $\Theta_{222,U}$ correspond to the baselines for the native and unfolded states, which have been approximated by the linear functions:

$$\Theta_{222,N} = a + b{\cdot}T \quad (2)$$

$$\Theta_{222,U} = c + d{\cdot}T \quad (3)$$

The thermodynamic enthalpy ($\Delta H_{N\text{-}U}$) and entropy ($\Delta S_{N\text{-}U}$) functions for the denaturation process are

$$\Delta H_{N-U} = \Delta H_{vH} + \Delta C_{pN-U}{\cdot}(T - T_m) \quad (4)$$

$$\Delta S_{N-U} = \Delta S_m + \Delta C_{pN-U}{\cdot}ln\left(\frac{T}{T_m}\right) \quad (5)$$

where the entropy change upon denaturation at T_m is $\Delta S_m = \Delta H_{vH}/T_m$ and the heat capacity change upon denaturation ($\Delta C_{pN\text{-}U}$) was taken to be independent of temperature.

Individual fittings of the experimental traces to the two-state model were performed taking T_m (the denaturation temperature, where the N and U populations are equal to 50 %), ΔH_{vH} (the denaturation enthalpy value, referenced at T_m), and the linear functions defining the ellipticity of the N and U states, to be floating parameters. In the initial stages of the analysis, $\Delta Cp_{N\text{-}U}$ was taken to be zero.

5.4. Differential scanning fluorimetry (DSF)

DSF measurements were followed in a in a CFX384 Touch Real-Time PCR Detection System (Bio-Rad, Hercules, CA), using a 384-well format. Syntenin-1, the tandem of PDZ domains, PDZ1 and PDZ2 thermal denaturation profiles were obtained recording the fluorescence intensity of SYPRO Orange using the HEX predefined filter (Ex/Em: 515–535/560–580 nm). DSF traces were generated at 1 $K{\cdot}min^{-1}$ ranging from 15 to 95 °C.

The assay was performed in 384-well format using Sarstedt PCR full

skirt, 384 well plates (Reference: 72.1984.202; Sarstedt, Nümbrecht, Germany). 10 μL reaction mixtures were set up in PBS pH 7.4, containing the Syntenin-1 protein or domains at 5, 20 or 50 μM and 5× concentration of SYPRO Orange (dilution from the 5000× commercial stock, Invitrogen, Waltham, MA).

Individual fittings of the unfolding traces to the two-state model were performed using the same protocol and equations than for the CD far-UV unfolding transitions.

CRediT authorship contribution statement

Jose C. Martinez: Software, Formal Analysis, Resources, Data Curation, Writing – Original Draft Preparation, Writing – Review & Editing, Visualization, Supervision. **Javier Ruiz-Sanz:** Methodology, Validation, Formal Analysis, Resources, Investigation, Writing – Review & Editing. **Maria J. Resina:** Methodology, Resources, Investigation. **Fernando Montero:** Methodology, Investigation, Validation. **Ana Camara-Artigas:** Software, Formal Analysis, Writing – Review & Editing. **Irene Luque:** Conceptualization, Writing – Review & Editing, Visualization, Supervision, Project Administration, Funding Acquisition.

Declaration of competing interest

The authors declare that they do not have conflicts of interest.

Acknowledgements

This research was funded by the Spanish Ministry of Education and Science [grants BIO2016-78746-C2-1-R and PID2020-112895RB-100]; the Junta de Andalucía (Andalusian Government, Spain) [grant BIO-18-UGR20]; and AEI/FEDER EU funds. A.C-A. also acknowledges funding by the Junta de Andalucía [grants UAL18-BIO-B005-B and PY20_00149]; and also AEI/FEDER EU funds. M.J.R. was recipient of a contract from the "Youth Guarantee Fund" program from the Andalusian Government. F.M. was recipient of a predoctoral fellowship from the Spanish Ministry of Education and Science. We thank the support of the C.I.C. of the University of Granada. Funding for open access charge: Universidad de Granada / CBUA.

Appendix A. Supplementary data

Supplementary data to this article can be found online at https://doi.org/10.1016/j.ijbiomac.2023.124662.

References

[1] D.B. Wetlaufer, Nucleation, rapid folding, and globular intrachain regions in proteins, Proc. Natl. Acad. Sci. 70 (3) (1973) 697–701, https://doi.org/10.1073/pnas.70.3.697.
[2] W. Pfeil, The problem of the stability globular proteins, Mol. Cell. Biochem. 40 (1) (1981) 3–28, https://doi.org/10.1007/bf00230185.
[3] P.L. Privalov, Stability of proteins.Proteins which do not present a single cooperative system, Adv. Protein Chem. 35 (1982) 1–104, https://doi.org/10.1016/S0065-3233(08)60468-4.
[4] P. Buzon, J. Ruiz-Sanz, J.C. Martinez, I. Luque, Stability, conformational plasticity, oligomerization behaviour and equilibrium unfolding intermediates of the Ebola virus matrix protein VP40, J. Biomol. Struct. Dyn. 38 (14) (2020) 4289–4303, https://doi.org/10.1080/07391102.2019.1671226.
[5] C. Tanford, Contribution of hydrophobic interactions to the stability of the globular conformation of proteins, J. Am. Chem. Soc. 84 (22) (1962) 4240–4247, https://doi.org/10.1021/ja00881a009.
[6] F. Ye, M. Zhang, Structures and target recognition modes of PDZ domains: recurring themes and emerging pictures, Biochem. J. 455 (1) (2013) 1–14, https://doi.org/10.1042/bj20130783.
[7] F. Delhommel, F. Cordier, B. Bardiaux, G. Bouvier, B. Colcombet-Cazenave, S. Brier, B. Raynal, S. Nouaille, A. Bahloul, J. Chamot-Rooke, M. Nilges, C. Petit, N. Wolff, Structural characterization of whirlin reveals an unexpected and dynamic supramodule conformation of its PDZ tandem, Structure 25 (11) (2017) 1645–1656, https://doi.org/10.1016/j.str.2017.08.013.
[8] D. Santorelli, L. Marcocci, V. Pennacchietti, C. Nardella, A. Diop, P. Pietrangeli, L. Pagano, A. Toto, F. Malagrinò, S. Gianni, Understanding the molecular basis of folding cooperativity through a comparative analysis of a multidomain protein and its isolated domains, J. Biol. Chem. 299 (3) (2023), https://doi.org/10.1016/j.jbc.2023.102983.
[9] C. Gautier, F. Troilo, F. Cordier, F. Malagrinò, A. Toto, L. Visconti, Y. Zhu, M. Brunori, N. Wolff, S. Gianni, Hidden kinetic traps in multidomain folding highlight the presence of a misfolded but functionally competent intermediate, Proc. Natl. Acad. Sci. 117 (33) (2020) 19963–19969, https://doi.org/10.1073/pnas.2004138117.
[10] L. Visconti, F. Malagrinò, F. Troilo, L. Pagano, A. Toto, S. Gianni, Folding and misfolding of a PDZ tandem repeat, J. Mol. Biol. 433 (7) (2021), 166862, https://doi.org/10.1016/j.jmb.2021.166862.
[11] L. Pagano, F. Malagrinò, L. Visconti, F. Troilo, V. Pennacchietti, C. Nardella, A. Toto, S. Gianni, Probing the effects of local frustration in the folding of a multidomain protein, J. Mol. Biol. 433 (15) (2021), 167087, https://doi.org/10.1016/j.jmb.2021.167087.
[12] F. Malagrinò, G. Fusco, V. Pennacchietti, A. Toto, C. Nardella, L. Pagano, A. de Simone, S. Gianni, Cryptic binding properties of a transient folding intermediate in a PDZ tandem repeat, Protein Sci. 31 (9) (2022), e4396, https://doi.org/10.1002/pro.4396.
[13] J.M. Beekman, P.J. Coffer, The ins and outs of syntenin, a multifunctional intracellular adaptor protein, J. Cell Sci. 121 (Pt 9) (2008) 1349–1355, https://doi.org/10.1242/jcs.026401.
[14] T. Shimada, S. Yasuda, H. Sugiura, K. Yamagata, Syntenin: PDZ protein regulating signaling pathways and cellular functions, Int. J. Mol. Sci. 20 (17) (2019), https://doi.org/10.3390/ijms20174171.
[15] L. Enjuanes, S. Zuniga, C. Castano-Rodriguez, J. Gutierrez-Alvarez, J. Canton, I. Sola, Molecular basis of coronavirus virulence and vaccine development, Adv. Virus Res. 96 (2016) 245–286, https://doi.org/10.1016/bs.aivir.2016.08.003.
[16] A.M. Wawrzyniak, E. Vermeiren, P. Zimmermann, Y. Ivarsson, Extensions of PSD-95/discs large/ZO-1 (PDZ) domains influence lipid binding and membrane targeting of syntenin-1, FEBS Lett. 586 (10) (2012) 1445–1451, https://doi.org/10.1016/j.febslet.2012.04.024.
[17] T. Cierpicki, J.H. Bushweller, Z.S. Derewenda, Probing the supramodular architecture of a multidomain protein: the structure of syntenin in solution, Structure 13 (2) (2005) 319–327, https://doi.org/10.1016/j.str.2004.12.014.
[18] A.Y. Hung, M. Sheng, PDZ domains: structural modules for protein complex assembly, J. Biol. Chem. 277 (8) (2002) 5699–5702, https://doi.org/10.1074/jbc.R100065200.
[19] P. Zimmermann, K. Meerschaert, G. Reekmans, I. Leenaerts, J.V. Small, J. Vandekerckhove, G. David, J. Gettemans, PIP(2)-PDZ domain binding controls the association of syntenin with the plasma membrane, Mol. Cell 9 (6) (2002) 1215–1225, https://doi.org/10.1016/s1097-2765(02)00549-x.
[20] B. Nal, C. Chan, F. Kien, L. Siu, J. Tse, K. Chu, J. Kam, I. Staropoli, B. Crescenzo-Chaigne, N. Escriou, S. van der Werf, K.Y. Yuen, R. Altmeyer, Differential maturation and subcellular localization of severe acute respiratory syndrome coronavirus surface proteins S,M and E, J. Gen. Virol. 86 (Pt 5) (2005) 1423–1434, https://doi.org/10.1099/vir.0.80671-0.
[21] J.L. Nieto-Torres, M.L. Dediego, E. Alvarez, J.M. Jimenez-Guardeno, J.A. Regla-Nava, M. Llorente, L. Kremer, S. Shuo, L. Enjuanes, Subcellular location and topology of severe acute respiratory syndrome coronavirus envelope protein, Virology 415 (2) (2011) 69–82, https://doi.org/10.1016/j.virol.2011.03.029.
[22] T.R. Ruch, C.E. Machamer, The coronavirus E protein: assembly and beyond, Viruses 4 (3) (2012) 363–382, https://doi.org/10.3390/v4030363.
[23] Y. Ye, B.G. Hogue, Role of the coronavirus E viroporin protein transmembrane domain in virus assembly, J. Virol. 81 (7) (2007) 3597–3607, https://doi.org/10.1128/JVI.01472-06.
[24] M.L. DeDiego, E. Alvarez, F. Almazan, M.T. Rejas, E. Lamirande, A. Roberts, W. J. Shieh, S.R. Zaki, K. Subbarao, L. Enjuanes, A severe acute respiratory syndrome coronavirus that lacks the E gene is attenuated in vitro and in vivo, J. Virol. 81 (4) (2007) 1701–1713, https://doi.org/10.1128/JVI.01467-06.
[25] M.L. Dediego, L. Pewe, E. Alvarez, M.T. Rejas, S. Perlman, L. Enjuanes, Pathogenicity of severe acute respiratory coronavirus deletion mutants in hACE-2 transgenic mice, Virology 376 (2) (2008) 379–389, https://doi.org/10.1016/j.virol.2008.03.005.
[26] C. Fett, M.L. DeDiego, J.A. Regla-Nava, L. Enjuanes, S. Perlman, Complete protection against severe acute respiratory syndrome coronavirus-mediated lethal respiratory disease in aged mice by immunization with a mouse-adapted virus lacking E protein, J. Virol. 87 (12) (2013) 6551–6559, https://doi.org/10.1128/JVI.00087-13.
[27] J. Netland, M.L. DeDiego, J. Zhao, C. Fett, E. Alvarez, J.L. Nieto-Torres, L. Enjuanes, S. Perlman, Immunization with an attenuated severe acute respiratory syndrome coronavirus deleted in E protein protects against lethal respiratory disease, Virology 399 (1) (2010) 120–128, https://doi.org/10.1016/j.virol.2010.01.004.
[28] J.M. Jimenez-Guardeno, J.L. Nieto-Torres, M.L. DeDiego, J.A. Regla-Nava, R. Fernandez-Delgado, C. Castano-Rodriguez, L. Enjuanes, The PDZ-binding motif of severe acute respiratory syndrome coronavirus envelope protein is a determinant of viral pathogenesis, PLoS Pathog. 10 (8) (2014), e1004320, https://doi.org/10.1371/journal.ppat.1004320.
[29] F. Conejero-Lara, P.L. Mateo, Presence of a slow dimerization equilibrium on the thermal unfolding of the 205–316 thermolysin fragment at neutral pH, Biochemistry 35 (11) (1996) 3477–3486, https://doi.org/10.1021/bi952358r.
[30] G.I. Makhatadze, P.L. Privalov, Heat capacity of proteins. I. Partial molar heat capacity of individual amino acid residues in aqueous solution: hydration effect, J. Mol. Biol. 213 (2) (1990) 375–384.

[31] P.L. Privalov, G.I. Makhatadze, Heat capacity of proteins. II. Partial molar heat capacity of the unfolded polypeptide chain of proteins: protein unfolding effects, J. Mol. Biol. 213 (2) (1990) 385–391.
[32] J. Murciano-Calles, E.S. Cobos, P.L. Mateo, A. Camara-Artigas, J.C. Martinez, An oligomeric equilibrium intermediate as the precursory nucleus of globular and fibrillar supramacromolecular assemblies in a PDZ domain, Biophys. J. 99 (1) (2010) 263–272, https://doi.org/10.1016/j.bpj.2010.04.003.
[33] S. Onchaiya, T. Saotome, K. Mizutani, J.C. Martinez, J.R.H. Tame, S.I. Kidokoro, Y. Kuroda, Reverse engineering analysis of the high-temperature reversible oligomerization and amyloidogenicity of PSD95-PDZ3, Molecules 27 (9) (2022), https://doi.org/10.3390/molecules27092813.
[34] T. Saotome, T. Mezaki, S. Brindha, S. Unzai, J.C. Martinez, S.I. Kidokoro, Y. Kuroda, Thermodynamic analysis of point mutations inhibiting high-temperature reversible oligomerization of PDZ3, Biophys. J. 119 (7) (2020) 1391–1401, https://doi.org/10.1016/j.bpj.2020.08.023.
[35] T. Saotome, S. Onchaiya, S. Brindha, T. Mezaki, S. Unzai, K. Noguchi, J. C. Martinez, S.I. Kidokoro, Y. Kuroda, Blocking PSD95-PDZ3's amyloidogenesis through point mutations that inhibit high-temperature reversible oligomerization (RO), FEBS J. 289 (11) (2022) 3205–3216, https://doi.org/10.1111/febs.16339.
[36] J. Murciano-Calles, J. Guell-Bosch, S. Villegas, J.C. Martinez, Common features in the unfolding and misfolding of PDZ domains and beyond: the modulatory effect of domain swapping and extra-elements, Sci. Rep. 6 (2016) 19242, https://doi.org/10.1038/srep19242.
[37] E. Freire, Differential scanning calorimetry, in: B.A. Shirley (Ed.), Protein Stability and Folding: Theory and Practice, Humana Press Inc., Totowa, NJ, 1995, pp. 191–218.
[38] E.S. Cobos, M. Iglesias-Bexiga, J. Ruiz-Sanz, P.L. Mateo, I. Luque, J.C. Martinez, Thermodynamic characterization of the folding equilibrium of the human Nedd4-WW4 domain: at the frontiers of cooperative folding, Biochemistry 48 (36) (2009) 8712–8720, https://doi.org/10.1021/bi9007758.
[39] A.R. Viguera, J.C. Martinez, V.V. Filimonov, P.L. Mateo, L. Serrano, Thermodynamic and kinetic analysis of the SH3 domain of spectrin shows a two-state folding transition, Biochemistry 33 (8) (1994) 2142–2150.
[40] B.S. Kang, D.R. Cooper, F. Jelen, Y. Devedjiev, U. Derewenda, Z. Dauter, J. Otlewski, Z.S. Derewenda, PDZ tandem of human syntenin: crystal structure and functional properties, Structure 11 (4) (2003) 459–468, https://doi.org/10.1016/s0969-2126(03)00052-2.
[41] J. Grembecka, T. Cierpicki, Y. Devedjiev, U. Derewenda, B.S. Kang, J. H. Bushweller, Z.S. Derewenda, The binding of the PDZ tandem of syntenin to target proteins, Biochemistry 45 (11) (2006) 3674–3683, https://doi.org/10.1021/bi052225y.
[42] R. Leblanc, R. Kashyap, K. Barral, A.L. Egea-Jimenez, D. Kovalskyy, M. Feracci, M. Garcia, C. Derviaux, S. Betzi, R. Ghossoub, M. Platonov, P. Roche, X. Morelli, L. Hoffer, P. Zimmermann, Pharmacological inhibition of syntenin PDZ2 domain impairs breast cancer cell activities and exosome loading with syndecan and EpCAM cargo, J. Extracell. Vesicles 10 (2) (2020), e12039, https://doi.org/10.1002/jev2.12039.
[43] A. Palencia, E.S. Cobos, P.L. Mateo, J.C. Martinez, I. Luque, Thermodynamic dissection of the binding energetics of proline-rich peptides to the Abl-SH3 domain: implications for rational ligand design, J. Mol. Biol. 336 (2) (2004) 527–537. S0022283603015341.
[44] A. Palencia, A. Camara-Artigas, M.T. Pisabarro, J.C. Martinez, I. Luque, Role of interfacial water molecules in proline-rich ligand recognition by the Src homology 3 domain of abl, J. Biol. Chem. 285 (4) (2010) 2823–2833, https://doi.org/10.1074/jbc.M109.048033.
[45] J.M. Martin-Garcia, J. Ruiz-Sanz, I. Luque, Interfacial water molecules in SH3 interactions: a revised paradigm for polyproline recognition, Biochem. J. 442 (2) (2012) 443–451, https://doi.org/10.1042/BJ20111089.
[46] M. Andujar-Sanchez, E.S. Cobos, I. Luque, J.C. Martinez, Thermodynamic impact of embedded water molecules in the unfolding of human CD2BP2-GYF domain, J. Phys. Chem. B 116 (24) (2012) 7168–7175, https://doi.org/10.1021/jp303495b.
[47] L.R. Olano, S.W. Rick, Hydration free energies and entropies for water in protein interiors, J. Am. Chem. Soc. 126 (25) (2004) 7991–8000, https://doi.org/10.1021/ja049701c.
[48] D.I. Paredes, K. Watters, D.J. Pitman, C. Bystroff, J.S. Dordick, Comparative void-volume analysis of psychrophilic and mesophilic enzymes: structural bioinformatics of psychrophilic enzymes reveals sources of core flexibility, BMC Struct. Biol. 11 (2011) 42, https://doi.org/10.1186/1472-6807-11-42.
[49] M. Iglesias-Bexiga, M. Szczepaniak, C. Sánchez de Medina, E.S. Cobos, R. Godoy-Ruiz, J.C. Martinez, V. Muñoz, I. Luque, Protein folding cooperativity and thermodynamic barriers of the simplest β-sheet fold: a survey of WW domains, J. Phys. Chem. B 122 (49) (2018) 11058–11071, https://doi.org/10.1021/acs.jpcb.8b05198.
[50] S. Fischer, C. Verma, R.E. Hubbard, Rotation of structural water inside a protein: calculation of the rate and vibrational entropy of activation, J. Phys. Chem. B 102 (1998) 1797–1805.
[51] A.E. Garcia, G. Hummer, Water penetration and escape in proteins, Proteins 38 (3) (2000) 261–272, https://doi.org/10.1002/(SICI)1097-0134.
[52] A.D. Robertson, K.P. Murphy, Protein structure and the energetics of protein stability, Chem. Rev. 97 (5) (1997) 1251–1268.
[53] Q. Zhang, J.S. Fan, M. Zhang, Interdomain chaperoning between PSD-95, Dlg, and Zo-1 (PDZ) domains of glutamate receptor-interacting proteins, J. Biol. Chem. 276 (46) (2001) 43216–43220, https://doi.org/10.1074/jbc.M105996200.
[54] W. Feng, Y. Shi, M. Li, M. Zhang, Tandem PDZ repeats in glutamate receptor-interacting proteins have a novel mode of PDZ domain-mediated target binding, Nat. Struct. Biol. 10 (11) (2003) 972–978, https://doi.org/10.1038/nsb992.
[55] F. Ye, Y. Huang, J. Li, Y. Ma, C. Xie, Z. Liu, X. Deng, J. Wan, T. Xue, W. Liu, M. Zhang, An unexpected INAD PDZ tandem-mediated plcβ binding in Drosophila photo receptors, eLife 7 (2018), e41848, https://doi.org/10.7554/eLife.41848.
[56] J.F. Long, W. Feng, R. Wang, L.N. Chan, F.C. Ip, J. Xia, N.Y. Ip, M. Zhang, Autoinhibition of X11/Mint scaffold proteins revealed by the closed conformation of the PDZ tandem, Nat. Struct. Mol. Biol. 12 (8) (2005) 722–728, https://doi.org/10.1038/nsmb958.
[57] S.T. Truschel, D. Sengupta, A. Foote, A. Heroux, M.R. Macbeth, A.D. Linstedt, Structure of the membrane-tethering GRASP domain reveals a unique PDZ ligand interaction that mediates golgi biogenesis, J. Biol. Chem. 286 (23) (2011) 20125–20129, https://doi.org/10.1074/jbc.C111.245324.
[58] J. Long, Z. Wei, W. Feng, C. Yu, Y.X. Zhao, M. Zhang, Supramodular nature of GRIP1 revealed by the structure of its PDZ12 tandem in complex with the carboxyl tail of Fras1, J. Mol. Biol. 375 (5) (2008) 1457–1468, https://doi.org/10.1016/j.jmb.2007.11.088.
[59] J. Ren, L. Feng, Y. Bai, H. Pei, Z. Yuan, W. Feng, Interdomain interface-mediated target recognition by the scribble PDZ34 supramodule, Biochem. J. 468 (1) (2015) 133–144, https://doi.org/10.1042/bj20141473.
[60] K.B. Nissen, L.M. Haugaard-Kedström, T.S. Wilbek, L.S. Nielsen, E. Åberg, A. S. Kristensen, A. Bach, P. Jemth, K. Strømgaard, Targeting protein-protein interactions with trimeric ligands: high affinity inhibitors of the MAGUK protein family, PLoS One 10 (2) (2015), e0117668, https://doi.org/10.1371/journal.pone.0117668.
[61] A. Toto, S.W. Pedersen, O.A. Karlsson, G.E. Moran, E. Andersson, C.N. Chi, K. Strømgaard, S. Gianni, P. Jemth, Ligand binding to the PDZ domains of postsynaptic density protein 95, Protein Eng. Des. Sel. 29 (5) (2016) 169–175, https://doi.org/10.1093/protein/gzw004.
[62] J.N. Eildal, A. Bach, J. Dogan, F. Ye, M. Zhang, P. Jemth, K. Strømgaard, Rigidified clicked dimeric ligands for studying the dynamics of the PDZ1-2 supramodule of PSD-95, Chembiochem 16 (1) (2015) 64–69, https://doi.org/10.1002/cbic.201402547.
[63] B. Kovács, N. Zajácz-Epresi, Z. Gáspári, Ligand-dependent intra- and interdomain motions in the PDZ12 tandem regulate binding interfaces in postsynaptic density protein-95, FEBS Lett. 594 (5) (2020) 887–902, https://doi.org/10.1002/1873-3468.13626.
[64] A. Krishnamohan, G.L. Hamilton, R. Goutam, H. Sanabria, F. Morcos, Coevolution and smFRET enhances conformation sampling and FRET experimental design in tandem PDZ1-2 proteins, J. Phys. Chem. B 127 (4) (2023) 884–898, https://doi.org/10.1021/acs.jpcb.2c06720.
[65] N. Calosci, C.N. Chi, B. Richter, C. Camilloni, Å. Engström, L. Eklund, C. Travaglini-Allocatelli, S. Gianni, M. Vendruscolo, P. Jemth, Comparison of successive transition states for folding reveals alternative early folding pathways of two homologous proteins, Proc. Natl. Acad. Sci. 105 (49) (2008) 19241–19246, https://doi.org/10.1073/pnas.0804774105.
[66] J. Murciano-Calles, J.C. Martinez, M. Marin-Argany, S. Villegas, E.S. Cobos, A thermodynamic study of the third PDZ domain of MAGUK neuronal protein PSD-95 reveals a complex three-state folding behavior, Biophys. Chem. 185 (2014) 1–7, https://doi.org/10.1016/j.bpc.2013.10.005.